

Anharmonicities in phonon combinations and overtones in bilayered graphene: A temperature-dependent approach

P. T. Araujo*

*Department of Physics and Astronomy, University of Alabama, Tuscaloosa, Alabama 35401, USA;
Center for Materials for Information Technology (MINT Center), University of Alabama, Tuscaloosa, Alabama 35401, USA;
and Natural Sciences Institute, Graduate Program in Physics, Federal University of Para, Belem, Pará, Brazil*



(Received 4 April 2018; published 25 May 2018)

This paper studies phonon anharmonicities related to the phonon combination LOZO' and phonon overtone 2ZO in a AB-stacked bilayer graphene (2LG). The results explain in detail the rule of the ZO' layer breathing mode in the 2LG electron and phonon relaxations, especially at temperatures above 543 K, where anomalous behaviors are observed for the LOZO' frequencies, linewidths (and therefore, lifetimes), and integrated areas. Surprisingly, the 2ZO frequencies and linewidths do not show any dependence with temperature (ZO is the out-of-phase vibration of the layers). This result is explained via nonsymmetric lattice distortions and via the almost null Grüneisen parameter associated to the ZO mode. Recently, the correct assignments for the phonon combination and overtone modes studied here have been put in debate once again in a theoretical work by Popov [Carbon **91**, 436 (2015)]. This work shows how temperature-dependent Raman spectroscopy is used to propose a solution for these recent assignment problems. Finally, although 2LG is the system used here, the measurements and discussions to approach electron and phonon relaxations have the potential to be extended to any other multilayered structure that presents ZO' - and ZO-like phonon modes.

DOI: [10.1103/PhysRevB.97.205441](https://doi.org/10.1103/PhysRevB.97.205441)

I. INTRODUCTION AND MOTIVATION

Phonons and phonon combinations play marginal roles in the description of electronic and thermal transport properties of materials [1–22], which are intimately connected to the equilibrium between the carriers loss (gain) of energy due to phonon emissions (absorptions) [1,9,16,23–26]. The efficiency of emission or absorption of phonons by a carrier will be directly connected with the time taken by an excited phonon to decay to its fundamental state (in other words, phonon lifetime) [1]. This decay process is often accomplished via three-phonon processes (called the Klemens' channel) and via four-phonon processes [1,2,5,6,11,12,15,23]. In these processes, excited phonons decay into combinations of acoustic phonons or acoustic and optical phonons, provided that conservation of energy and momentum exists. Temperature-dependent phenomena are ruled by anharmonic phonon-phonon ($ph-ph$) couplings, also driven by three- and four-phonon processes, and by electron-phonon ($e-ph$) couplings, in which electrons will either absorb or emit a phonon [1,2,27,28]. In this context, it is paramount to assign phonons in materials, understand their symmetry, their coupling to electronic states, how they couple to each other and, finally, how these couplings depend on the temperature (T) and Fermi level energy (E_F). The lifetime of electrons and phonons in carbon materials has been probed by a plethora of techniques such as transient absorption spectroscopy [16,26], optical pump-probe [11,29,30], and terahertz techniques [31–34]. It is true, however, that understanding of decay pathways in carbon materials [especially their two-dimensional (2D) versions] is not complete.

The layers in multilayer 2D-materials (ML-2D) are connected to each other via interlayer (IEL) interactions mediated by van der Waals (vdW) forces, which are weak forces when compared with the intralayer (IAL) interactions mediated by covalent forces [3,4,35–38]. We may categorize phonons in ML systems in two groups: low-energy interlayer phonons (ph_{IEL}) and intralayer phonons (ph_{IAL}). Usually, ph_{IEL} have energies ranging from 0.6 to 12 meV, which are in the infrared (IR) range of energies [25,39–45]. Therefore, understanding ph_{IEL} becomes naturally important for developing 2D materials for IR optics and telecommunications. These ph_{IEL} are also important for relaxation mechanisms as they offer different relaxation pathways for excited phonons and electrons [7,9,11,25,46–49]. Due to its versatility, which includes possibilities for tunable band-gap and IEL interactions [39,49–51], bilayer graphene (2LG) is a model for van der Waals structures. Phonon combinations and overtones involving ph_{IEL} , which appears between 1600 and 1800 cm^{-1} in the Raman spectrum [see Fig. 1(a)] [39,42,43,50,52], are spectroscopic signatures for 2LG and their contributions to the 2LG properties must be properly addressed.

The Raman peaks in this spectral range have been assigned to the phonon combination LOZO' and to the phonon overtone 2ZO, both occurring at the Γ point, in which LO is the longitudinal optical mode (with frequency $\omega_{LO} = 1575 \text{ cm}^{-1}$ predicted at the Γ point), ZO' is the 2LG interlayer breathing mode (with frequency $\omega_{ZO'} = 90 \text{ cm}^{-1}$ predicted at the Γ point), and ZO is the out-of-plane tangential optical mode (with frequency $\omega_{ZO} = 885 \text{ cm}^{-1}$ predicted at the Γ point) [39,42,43,52]. Figure 1(b) shows the phonon dispersion for a 2LG in which the phonons mentioned above are labeled. Although these combination and overtone modes are reported

*paulo.t.araujo@ua.edu

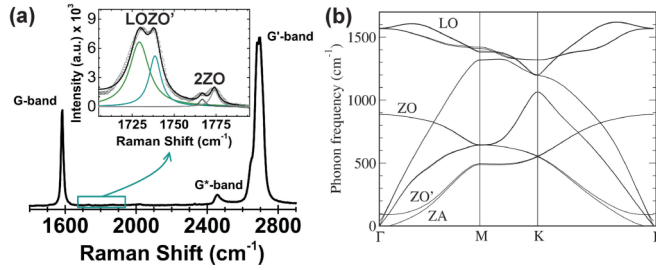


FIG. 1. (a) An example of Raman spectrum exhibiting the G^- , G^* , and G' (or 2D) bands. The inset shows the spectrum zoomed in the spectral region referent to the phonon combination LOZO' and 2ZO phonon overtone. (b) Phonon dispersion for bilayer graphene (2LG) showing the LO phonon mode (1575 cm^{-1} at the Γ point), the ZO phonon mode (885 cm^{-1} at the Γ point), the ZO' phonon mode (90 cm^{-1} at the Γ point), and the ZA phonon mode (0 cm^{-1} at the Γ point) [39,40].

in the literature [39,42,43,52], many aspects of their e - ph and ph - ph interactions have yet to be understood. The assignments given to these Raman spectral features need further confirmation as well: (1) Due to the IEL the LO mode in 2LG presents an antisymmetric component ($\text{LO}^{(-)}$) and a symmetric component ($\text{LO}^{(+)}$) [13,52–55], which means that the LO mode in the combination LOZO' needs to be assigned to either $\text{LO}^{(-)}$ or $\text{LO}^{(+)}$. (2) Popov [55], in disagreement with Lui *et al.* [42,43] and Sato *et al.* [52], has theoretically reassigned the 2ZO overtone to the phonon combination $\text{TO}^{(+)}\text{ZO}'$ at the K point, in which $\text{TO}^{(+)}$ stands for symmetric transverse-optical mode. Recently, Araujo *et al.* [39], explored the phonon self-energy renormalizations for the LOZO' and 2ZO peaks using gate-modulated Raman spectroscopy but, to the best of the author's knowledge, a detailed temperature-dependent study for such spectral features is still elusive. Exploration of temperature-dependent phenomena is fundamental to understand phonon anharmonicities involving ph_{IEL} and ph_{IAL} in a 2LG as well as in other layered systems [7,9,11,25,27,29,30,46–49,56]. Note that features such as the G band and the G' band (or 2D band) have already been explored for temperatures ranging from 4.2 to 475 K [8,17,18,27,28,57–62].

Any layered material with layers connected by vdW forces will present ZO'-like phonons (breathing modes) [25,39–45]. Such breathing modes are low-energy optical phonons with features that resemble flexural acoustic phonons [25]. Therefore, they will offer additional relaxation pathways for excited phonons [7,9,11,25,27,29,30,46–49,56]. In fact, these phonons are expected to play important roles at high temperatures, and they are also expected to strongly couple to ph_{IAL} modes [7,25,30,46,48,56]. In graphite, it is known that the ZO' phonon strongly couples to the infrared active mode $\text{LO}^{(-)}$ with frequency around 1590 cm^{-1} at the Γ point [60]. It has also been suggested that, at high temperatures, the ZO' mode strongly influences the spectral line shape of the G' band (also known as the 2D band) in a 2LG [40]. In this paper, 2LG is used as a template to explore the contributions of ph_{IEL} in relaxation processes involving electrons and phonons in a 2D system. Temperature-dependent Raman-scattering measurements in a broad range of temperatures (from 300 to 810 K) are performed to study phonon frequencies (ω_{ph}),

linewidths (Γ_{ph}), and integrated areas (IA_{ph}) of the Raman features LOZO' and 2ZO. The results are interesting and show a unexpected behavior associated to the combination mode LOZO' for temperatures above 543 K. At lower temperatures ($T < 543 \text{ K}$) the three-phonon relaxation processes involving the LO and the ZO' modes dominate but, at high temperatures ($T > 543 \text{ K}$), the four-phonon relaxation process and the ZO' mode itself become fundamental to explain the anharmonicities and relaxation dynamics observed. Additionally, the temperature-dependent results for the 2ZO phonon do not show such unexpected behavior and do not clearly present three- and four-phonon processes either.

II. EXPERIMENTAL DETAILS

A. Experimental measurements

Raman measurements were taken in the back scattering configuration using a Nd:YAG laser with excitation energy (E_L) 2.33 eV (532 nm). The temperature was varied using two different approaches: (1) by changing the laser power density in the range from 0.5 to $12 \text{ mW}/\mu\text{m}^2$; and (2) by keeping the laser power density low enough to avoid laser-related heat effects and changing the temperatures in a microscope cryostat where the temperatures could be controlled. The temperature was also checked against a simple blackbody model by following the method by Balkanski *et al.* [5]. The sample was exposed to the laser beam, whose spot size was $\sim 1 \mu\text{m}$ with a $100\times$ objective. In this range of power densities (0.5 – $12 \text{ mW}/\mu\text{m}^2$) and temperatures (300–810 K), no D band was observed in the Raman spectra, indicating that no disorder or defects were introduced by the laser light exposure. The measurements were done on exfoliated 2LG samples produced by the micromechanical cleavage of graphite on a Si substrate covered with 300 nm of SiO_2 [63]. The 2LG flakes were identified by the color contrast in an optical microscope, followed by Raman spectroscopy characterization [35]. All the Raman features presented in the measured spectra were fitted with Lorentzian curves.

B. Experimental data description

Figure 2(a) shows the phonon combination LOZO' and the overtone 2ZO in greater detail including the Lorentzian curves associated to each Raman peak. The LOZO' arises from a non-null momentum ($q \neq 0$) intravalley (AV) double-resonance process at the Γ point and it splits in two peaks, the $\text{LOZO}^{(+)}$ (from now on M_{11}) and the $\text{LOZO}^{(-)}$ (from now on, M_{22}), whose frequency dispersions are $\partial\omega_{M_{11}}/\partial E_L = 55.1 \text{ cm}^{-1}/\text{eV}$ and $\partial\omega_{M_{22}}/\partial E_L = 34.2 \text{ cm}^{-1}/\text{eV}$ [39,42,43,52]. The splitting observed for the LOZO' combination mode does not come from the phonon dispersion [see Fig. 1(b)], but instead, it comes from different resonant regimes involving the electronic valence (π_1 and π_2) and conduction (π_1^* and π_2^*) bands of the 2LG [39,42,43,52]. As shown in Fig. 2(b), the M_{11} peak arises from a double-resonance process involving the $\pi_1(\pi_1^*)$ bands and the M_{22} peak arises from a double-resonance process involving the $\pi_2(\pi_2^*)$ bands. These resonance conditions require the phonon momentum q for the M_{11} mode to be larger than that for the M_{22} mode ($q_{M_{11}} > q_{M_{22}}$) [39,42,43,52]. As a consequence the

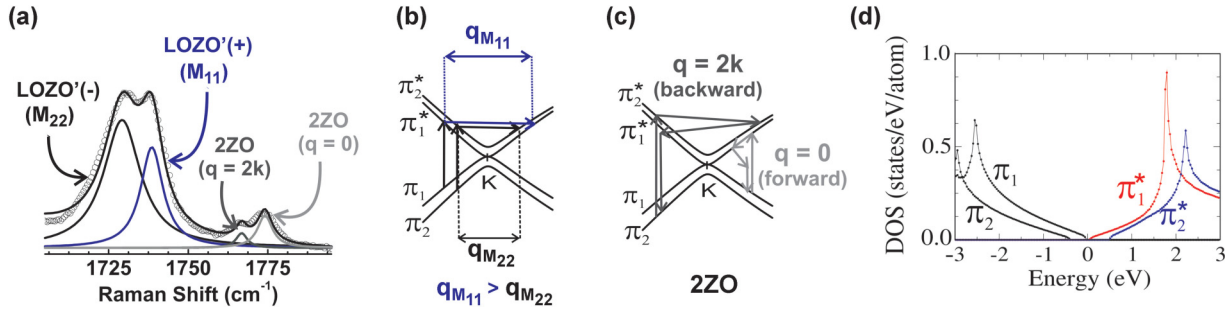


FIG. 2. (a) Raman peaks showing the LOZO' phonon combination and 2ZO phonon overtone features. The peaks are fitted using Lorentzian curves as shown in the figure. (b) The LOZO' mode is resonant with both electronic bands; the π_1 (π_1^*), giving rise to the M_{11} peak and the π_2 (π_2^*) giving rise to the M_{22} peak. Note that $q_{M_{11}} > q_{M_{22}}$ implying that $\omega_{M_{11}} > \omega_{M_{22}}$. (c) Backward ($q = 2k$) and forward ($q = 0$) scattering processes giving rise to the peaks $2ZO_{q=2k}$ and $2ZO_{q=0}$ as shown in (a). (d) Density of electronic states of 2LG for the valence bands π_1 and π_2 (black curves) and for the conduction bands π_1^* (red curve) and π_2^* (blue curve) [39,40].

phonon energies are such that $\hbar\omega_{M_{11}} > \hbar\omega_{M_{22}}$. The overtone 2ZO also splits into two features [see Fig. 2(c)]: one is related to a zero momentum ($q = 0$) AV forward scattering process ($2ZO_{q=0}$) at the Γ point and the other is related to a $q \neq 0$ AV backward scattering process ($2ZO_{q=2k}$) also at the Γ point [39,52]. The peak $2ZO_{q=2k}$ presents negative energy dispersion $\partial\omega_{2ZO_{q=2k}}/\partial E_L = -48.1 \text{ cm}^{-1}/\text{eV}$ but the peak $2ZO_{q=0}$ presents no dispersion [39,52].

Figures 3(a)–3(c) show, respectively, integrated areas ($IA_{M_{ii}}$ for $i = 1, 2$), linewidths ($\Gamma_{M_{ii}}$ for $i = 1, 2$), and frequency variations ($\Delta\omega_{M_{ii}}$ for $i = 1, 2$) for the combination LOZO' (M_{11} and M_{22} peaks) with increasing temperature (T). It is clear that two regimes, $T < 543 \text{ K}$ and $T \geq 543 \text{ K}$ exist. In the regime $T < 543 \text{ K}$, the results follow trends that have already been discussed in the literature for other modes such as the G and G' phonon modes [8,17,18,27,28,57–62]. In the regime

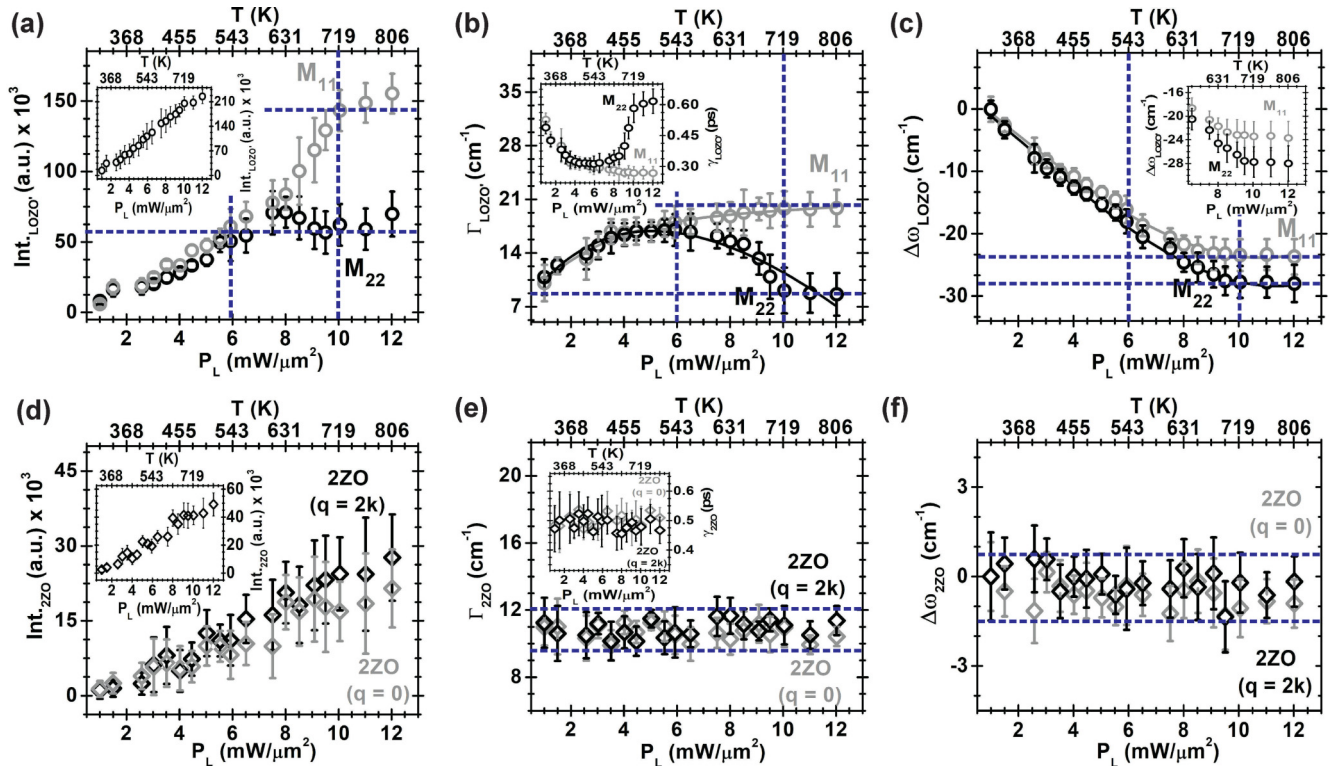


FIG. 3. (a) Raman integrated areas $IA_{M_{11}}$ and $IA_{M_{22}}$ as a function of both laser power density (P_L) and temperature (T). The inset corresponds to the total integrated area. (b) The evolution of the M_{11} and M_{22} linewidths ($\Gamma_{M_{11}}$ and $\Gamma_{M_{22}}$) with increasing T (P_L). The inset shows the phonon's lifetime ($\gamma_{M_{ii}} = \hbar/\Gamma_{M_{ii}}$ for $i = 1, 2$). (c) M_{11} and M_{22} frequency variations $\Delta\omega_{M_{ii}} = \omega_{M_{ii}} - \omega_{M_{ii}}^0$ (for $i = 1, 2$) with increasing T (P_L), where $\omega_{M_{ii}}^0$ is the frequency at room temperature. The inset is a zoom at higher temperatures. (d) Raman integrated areas $IA_{2ZO_{q=2k}}$ and $IA_{2ZO_{q=0}}$ as a function of both P_L and T . Once again the inset corresponds to the total integrated area. (e) The evolution of the $2ZO_{q=2k}$ and $2ZO_{q=0}$ linewidths ($\Gamma_{2ZO_{q=2k}}$ and $\Gamma_{2ZO_{q=0}}$) with increasing T (P_L). The inset shows the phonon's lifetime ($\gamma_{2ZO_{q=2k(q=0)}} = \hbar/\Gamma_{2ZO_{q=2k(q=0)}}$). (f) $2ZO_{q=2k}$ and $2ZO_{q=0}$ frequency variations $\Delta\omega_{2ZO_{q=2k(q=0)}} = \omega_{2ZO_{q=2k(q=0)}} - \omega_{2ZO_{q=2k(q=0)}}^0$ with increasing T (P_L), where $\omega_{2ZO_{q=2k(q=0)}}^0$ is the frequency at room temperature. The navy dashed lines are guides to the eyes.

$T \geq 543$ K, unexpected trends manifest as the temperature further increases. Regarding the 2ZO overtone, Figs. 3(d)–3(f) show, respectively, integrated areas ($IA_{2ZO_{q=0}}$ and $IA_{2ZO_{q=2k}}$), linewidths ($\Gamma_{2ZO_{q=0}}$ and $\Gamma_{2ZO_{q=2k}}$), and frequency variations ($\Delta\omega_{2ZO_{q=0}}$ and $\Delta\omega_{2ZO_{q=2k}}$) with increasing the temperature. Contrarily to what is seen for the LOZO' peaks, no significant variations for linewidths and frequencies are observed and relatively small variations for IAs are measured.

III. THEORETICAL BACKGROUND

The temperature dependence of a phonon frequency is well described as a result of two additive phenomena: lattice thermal expansion and phonon anharmonicities (*ph-ph* couplings). By taking both effects into account, the temperature-dependent frequency shift for a particular phonon mode will be written as [1,2,5,6,8,12,15,17,23,27,28,58,60]

$$\Delta\omega_{\text{mode}} = \Delta\omega_{LE}(T) + \Delta\omega_{ph-ph}^{\text{mode}}(T), \quad (1)$$

where the shift due to thermal expansion is given by

$$\Delta\omega_{LE}(T) = \omega_0 \left[\exp\left(-\delta_{\text{mode}}^{\text{out}} \int \alpha_{\text{out}}(T') dT'\right) - 2\delta_{\text{mode}}^{\text{in}} \int \alpha_{\text{in}}(T') dT'\right] - 1, \quad (2)$$

and the shift due to anharmonic effects is given by

$$\begin{aligned} \Delta\omega_{ph-ph}^{\text{mode}}(T) &= C_{\text{mode}}^{3-ph} \left[1 + \sum_{j=1}^2 \frac{1}{(e^{x_j} - 1)} \right] \\ &+ C_{\text{mode}}^{4-ph} \left[1 + \sum_{j=1}^3 \left(\frac{1}{(e^{y_j} - 1)} + \frac{1}{(e^{y_j} - 1)^2} \right) \right]. \quad (3) \end{aligned}$$

In Eq. (2), $\delta_{\text{mode}}^{\text{in}}$ ($\delta_{\text{mode}}^{\text{out}}$) is the phonon-dependent 2LG in-plane (out-of-plane) Grüneisen parameter and $\alpha_{\text{in}}(T)$ [$\alpha_{\text{out}}(T)$] is the 2LG in-plane (out-of-plane) coefficient of thermal expansion, which are well documented in the literature [6,8,9,17,22]. The in-plane temperature parameters are considered isotropic [1,6,8,9,17,22]. The first term in Eq. (3) refers to an anharmonic process (also known as a three-phonon process) that couples an optical phonon to two other phonons, and the second term refers to an anharmonic process (also known as a four-phonon process) that couples an optical phonon to three other phonons [1,2,5,6,8,12,15,17,23,27,28,58,60]. The three-phonon process usually follows the Klemens' decay channel in which one optical phonon decays emitting two acoustic phonons [1,2]. The constants C_{mode}^{3-ph} and C_{mode}^{4-ph} are fitting parameters which give the weight of each contribution in the anharmonic processes. Since momentum and energy are expected to conserve, in Eq. (3) $x_1 + x_2 = \hbar\omega_0/k_bT$ and $y_1 + y_2 + y_3 = \hbar\omega_0/k_bT$. The *ph-ph* couplings ruling the three-phonon and four-phonon processes depend on the Grüneisen parameter (δ_{mode}) as well: the probability for these couplings to happen is proportional to δ_{mode}^2 . The frequency shift $\Delta\omega_{\text{mode}}$ described in Eq. (1) must still take into account frequency shifts related to the strain effect caused by the

mismatch between the thermal expansion for SiO_2 and for the 2LG, which is described by

$$\Delta\omega_S(T) = \beta_{\text{mode}} \int [\alpha_{\text{SiO}_2}(T') - \alpha_{2\text{LG}}(T')] dT', \quad (4)$$

where β_{mode} is the biaxial coefficient related to a given phonon mode in 2LG, and α_{SiO_2} and $\alpha_{2\text{LG}} = \alpha_{\text{in}} + \alpha_{\text{out}}$ are, respectively, the thermal coefficient expansion for SiO_2 and 2LG graphene. The contributions coming from Eq. (4) are considered in the analysis presented here but they are very small for 2LG in the range of temperatures used in the experiments. When compared with 1LG, 2LG is much more robust and less susceptible to changes due to lattice mismatch [9,11,17,56,59].

The phonon linewidth (Γ) also depends on the *e-ph* and *ph-ph* interactions. The dependence of Γ with the temperature, $\Delta\Gamma_{\text{mode}}$, will be given by [1,2,5,6,8,12,15,17,23,27,28,58,60]:

$$\Delta\Gamma_{\text{mode}} = \Delta\Gamma_{e-ph}(T) + \Delta\Gamma_{ph-ph}^{\text{mode}}(T), \quad (5)$$

where the *e-ph* contribution is given by

$$\Delta\Gamma_{e-ph}(T) = \Gamma(0) \left[f\left(-\frac{\hbar\omega_0}{2k_bT}\right) - f\left(\frac{\hbar\omega_0}{2k_bT}\right) \right], \quad (6)$$

and the *ph-ph* contribution is written as

$$\begin{aligned} \Delta\Gamma_{ph-ph}^{\text{mode}}(T) &= D_{\text{mode}}^{3-ph} \left[1 + \sum_{j=1}^2 \frac{1}{(e^{x_j} - 1)} \right] \\ &+ D_{\text{mode}}^{4-ph} \left[1 + \sum_{j=1}^3 \left(\frac{1}{(e^{y_j} - 1)} + \frac{1}{(e^{y_j} - 1)^2} \right) \right]. \quad (7) \end{aligned}$$

Once again, the first term in Eq. (7) refers to an anharmonic process that couples an optical phonon to two phonons (three-phonon process) and the second term refers to an anharmonic process that couples an optical phonon to three phonons (four-phonon process). Equation (6) describes the change in the phonon lifetime related to the creation (annihilation) of *e-ph* pairs due to phonon absorption (emission). Note that, in Eq. (6), $f(x) = 1/[\exp(x) + 1]$ is the Fermi-Dirac distribution [10,27,28].

As a first approximation, the integrated area (IA) in a Raman-scattering event is ruled by its Raman cross section $\sigma_{ij}^{\text{mode}}$, which is proportional to the product $\mathbf{H}_{ij} \times \mathbf{Q}_{ij}^{\text{mode}}$ (for $i = 1, 2$ and $j = 1, 2$). \mathbf{H}_{ij} gives the electron-photon (*e-p*) coupling and $\mathbf{Q}_{ij}^{\text{mode}}$ gives the *e-ph* coupling between electrons and phonons [39,40,52]. Due to symmetry requirements \mathbf{H}_{ij} comes from π_i to π_i^* (for $i = 1, 2$) vertical transitions between electronic states [39,40,54,55]. For the LOZO' peaks, $\mathbf{Q}_{ii}^{\text{M}_{11}} (\mathbf{Q}_{ii}^{\text{M}_{22}})$ describes the scattering of an electron by a phonon from π_i^* to π_i^* (for $i = 1, 2$); on the other hand, for the 2ZO peaks, $\mathbf{Q}_{ij}^{2ZO_{q=0}} (\mathbf{Q}_{ij}^{2ZO_{q=2k}})$ describes the scattering of an electron by a phonon from π_i^* to π_j^* (for $i, j = 1, 2$). Theoretical calculations by Popov [55] and Sato *et al.* [52] suggest that (1) $\sigma_{11}^{\text{M}_{11}} \approx \sigma_{22}^{\text{M}_{22}}$, and (2) that $\sigma_{12}^{2ZO_{q=0}} (\sigma_{21}^{2ZO_{q=0}}) \approx \sigma_{12}^{2ZO_{q=2k}} (\sigma_{21}^{2ZO_{q=2k}})$. For the overtone 2ZO, the calculations did not explicitly consider differences between a phonon scattering from π_1^* to π_2^* or from

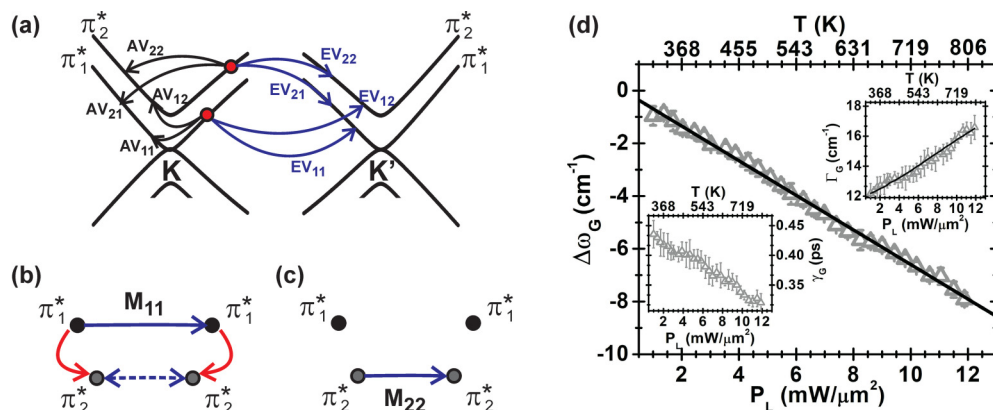


FIG. 4. (a) Possible intravalley (AV) or intervalley (EV) electron relaxation processes by the emission of a phonon (the same processes can also occur by the absorption of a phonon). Panels (b) and (c) show, respectively, the possible π_1^* to π_2^* net electron relaxation channels (red solid arrows) associated to the Raman-scattering processes generating the peaks M_{11} and M_{22} . The navy solid arrows represent the original electron scattering events for M_{11} (b) and M_{22} (c). The dashed lines represent the new possible scattering processes for the electron after the relaxation. In this sense, from the most to the least favored process by electron relaxation we have $M_{22} > M_{11}$. (d) G -band frequency variation $\Delta\omega_G = \omega_G - \omega_G^0$ with increasing temperature, where ω_G^0 is the frequency at room temperature. The black solid line is the fitting result using the relation $\Delta\omega_G = \chi_G T$, where $\chi_G = 1.56 \times 10^{-2} \text{ cm}^{-1}/\text{K}$. The inset in the upper-right corner shows the evolution of the G -band linewidth (Γ_G) with increasing temperature [the black solid line is the fitting result using Eq. (7)], while the inset in the lower-left corner shows the phonon's lifetime ($\gamma_G = \hbar/\Gamma_G$) evolution with increasing temperature.

π_2^* to π_1^* . However, by taking into account symmetry considerations [39,40,54,55] and by considering similar scattering processes that are extensively studied in the literature, such as those ruling the G' (or 2D) band [with the exception that the G' is an intervalley (EV) process] [35,40,50,64], it is hypothesized that the scattering events from π_1^* to π_2^* or from π_2^* to π_1^* will have approximately the same contribution for the 2ZO peaks and that $q_{12} \approx q_{21}$ for $q_{ij} = 2k$ ($i = 1, 2$ and $j = 1, 2$). It is known from the literature that $\mathbf{H}_{11} > \mathbf{H}_{22}$, which implies that $\mathbf{Q}_{11}^{M_{11}} < \mathbf{Q}_{22}^{M_{22}}$ and $\mathbf{Q}_{12}^{2ZO_{q=0}} (\mathbf{Q}_{12}^{2ZO_{q=2k}}) \approx \mathbf{Q}_{21}^{2ZO_{q=0}} (\mathbf{Q}_{21}^{2ZO_{q=2k}})$ [39,40,52,55]. The temperature dependence of the IAs is ruled by the Bose-Einstein distribution for phonons and by the Fermi-Dirac distribution for electrons [1,65,66].

IV. RESULTS AND DISCUSSION

A. LOZO' integrated areas ($\text{IA}_{M_{11}}$ and $\text{IA}_{M_{22}}$)

Figure 3(a) shows the temperature dependence of the M_{11} and M_{22} integrated areas ($\text{IA}_{M_{11}}$ and $\text{IA}_{M_{22}}$, respectively) with increasing the temperature T (or laser power density P_L). It is seen that both $\text{IA}_{M_{11}}$ and $\text{IA}_{M_{22}}$ increase monotonically at similar rates in the range of temperatures from 300 to 543 K. However, for temperatures above 543 K ($T \geq 543$ K) $\text{IA}_{M_{11}}$ and $\text{IA}_{M_{22}}$ split and while $\text{IA}_{M_{11}}$ continues to increase with increasing T , $\text{IA}_{M_{22}}$ seems to present a stationary behavior. As mentioned above, $\text{IA}_{M_{11}}$ and $\text{IA}_{M_{22}}$ arise from AV double-resonance scattering [39,42,43,52]: an electron is photoexcited from the valence band to the conduction band and then it is scattered by a LO (or ZO') phonon to another electronic state in the opposite side of the electronic dispersion [see Fig. 2(b)] and then it is scattered back by a ZO' (or LO) phonon. Before the scattering by a phonon occurs, the photoexcited electron can relax from π_1^* to π_2^* (or from π_2^* to π_1^*) by either emitting or absorbing a low-energy phonon (usually an acoustic phonon) [40,47,67]. Such relaxations will also involve

intraband ($\pi_i^* \leftrightarrow \pi_i^*$) and interband processes ($\pi_i^* \leftrightarrow \pi_j^*$), as shown in Fig. 4(a). It is known that in the range of laser excitation energies (E_L) from 2.00 to 3.00 eV ($E_L = 2.33$ eV in this work) the electron relaxation time is about one order of magnitude faster via the emission of a phonon than via the absorption of phonon [47,67]. This is reasonable since emission does not require a phonon to be available in the material but absorption does [40,47,67]. The relaxation rates are proportional to density of states (DOS) [40,47,67], and for the range of energies aforementioned, the DOS for the π_1^* [red curve in Fig. 2(d)] is always larger than the DOS for the π_2^* [blue curve in Fig. 2(d)]. This means that a lower relaxation rate from π_2^* to π_1^* is expected in comparison with the relaxation rate from π_1^* to π_2^* , which leads to a net electron relaxation from π_1^* to π_2^* . Similar relaxation processes have been comprehensively addressed for the G' band [40].

Figure 4(a) illustrates the possible electron relaxation processes affecting the scattering events that generate M_{11} and M_{22} . The navy solid arrow and the red solid arrows in Fig. 4(b) illustrate, respectively, the original scattering events and the net relaxation from π_1^* to π_2^* . The dashed double-sided arrow illustrates the new scattering process which originates from such net relaxations. These net relaxations from π_1^* to π_2^* make the rate of the electronic scattering which generates M_{11} decrease (causing a decrease of its IA) and contribute to an increase in the rate of electronic scattering which generates M_{22} (causing an increase of its IA). As illustrated in Fig. 4(c), scattering events that generate M_{22} do not contribute to M_{11} because the net relaxation is from π_1^* to π_2^* . For $T < 543$ K, it is seen that the IAs for both peaks increase smoothly, which points towards a prevalence of a good balance between the net π_1^* to π_2^* electron relaxations and the electronic scattering that generates the LOZO' peaks. As shown in Fig. 3(a), for $T \geq 543$ K the rate with which $\text{IA}_{M_{11}}$ increases with increasing T becomes slightly different from the rate observed for $\text{IA}_{M_{22}}$. Note that the higher the temperature, the larger

the differences between $IA_{M_{11}}$ and $IA_{M_{22}}$. Specifically, while $IA_{M_{11}}$ continues to increase smoothly, $IA_{M_{22}}$ stops increasing and becomes nearly constant, which suggests that a stationary regime is taking place. This is understood as follows: (1) by increasing the temperature, the $\pi_1^* \rightarrow \pi_2^*$ net relaxation rate of photoexcited electrons via acoustic-phonon emission increases and the relaxation rate of optical phonons generated in the electronic scattering from $\pi_1^* \rightarrow \pi_1^*$ (M_{11} peak) and from $\pi_2^* \rightarrow \pi_2^*$ (M_{22} peak) into acoustic phonons via three-phonon and four-phonon processes also increases; (2) as previously suggested by Mafra *et al.* [40] and corroborated here, the combination of higher temperatures with the specific $E_L = 2.33$ eV leads to an extra interband relaxation mechanism mediated by ZO' phonons [40,47,67]. With a more efficient $\pi_1^* \rightarrow \pi_2^*$ electron relaxation (and an inefficient $\pi_2^* \rightarrow \pi_1^*$ relaxation) the generation of excited electrons in the π_2^* band is higher than the scattering and relaxation rates of such electrons by emission of optical (via $\pi_2^* \rightarrow \pi_2^*$ scattering) and acoustic phonons (via three- and four-phonon processes). $IA_{M_{11}}$ does not reach such a stationary regime because the generation of excited electrons in π_1^* is lower than the respective electronic scattering and relaxation rates. As shown in the inset of Fig. 3(a), the total IA ($IA_{M_{11}} + IA_{M_{22}}$) increases monotonically as the temperature increases, which means that the processes ruling the changes in the IAs are continuous and come from electron and phonon relaxations involving M_{11} and M_{22} combination modes.

It is important to note that for $T \geq 719$ K the rate with which $IA_{M_{11}}$ increases with increasing the temperature is smaller when compared to the same rate at $T < 719$ K. It is also seen that $IA_{M_{22}}$ seems to start increasing again for $T \geq 719$ K and it is no longer in a stationary regime. These new changes in behavior observed for both $IA_{M_{11}}$ and $IA_{M_{22}}$ are expected and understood as follows: for $T < 719$ K, as discussed above, there is a net relaxation from $\pi_1^* \rightarrow \pi_2^*$ via phonon emissions. However, in order for an efficient net $\pi_1^* \rightarrow \pi_2^*$ relaxation to exist, the phonon relaxation rates must be higher than the phonon generation rates [1,7,9,11,16,23–27,29,30,46–49,56,67]. If the generation of phonons is as efficient as the relaxation of phonons, an electron relaxing from $\pi_1^* \rightarrow \pi_2^*$ via phonon emission could reabsorb the same type phonon before it decays. In this case, phonons and electrons would become long-lived as they would reach thermal equilibrium. Since the stationary regime observed for $IA_{M_{22}}$ is caused by an extra channel created via ZO' relaxations [40,47,67], it is likely that the generation of ZO' becomes more efficient as the temperature increases as well, which is in accordance with the literature [11,16,25,26]. In this scenario, the relaxation rates for the ZO' phonons would be balanced by the generation rates of such a phonon, which would lead to a loss of efficiency in the net relaxation of electrons from $\pi_1^* \rightarrow \pi_2^*$. With less relaxation pathways, the Raman scattering processes involving the ZO' phonon (such as the LOZO' combination) would lose efficiency. Moreover, it is known that scattering events involving absorption of phonons such as the Raman anti-Stokes scattering [5,65,66,69] become more effective with increasing temperature. Therefore, the results indicate that for $T \geq 719$ K $\pi_i^* \rightarrow \pi_i^*$ (for $i = 1,2$) electron scattering via phonon absorption becomes efficient, which means that electronic scattering events in-

volving phonons absorption and emission tend to become balanced.

B. LOZO' linewidths ($\Gamma_{M_{11}}$ and $\Gamma_{M_{22}}$)

Figure 3(b) shows the evolution of the LOZO' linewidths ($\Gamma_{M_{11}}$ and $\Gamma_{M_{22}}$) with increasing temperature. Once again, it is seen that for $T < 543$ K the two curves seem to overlap each other but for $T \geq 543$ K, $\Gamma_{M_{11}}$ continues to increase until it reaches $T = 719$ K when the curve seems to become stationary. On the other hand, $\Gamma_{M_{22}}$ starts decreasing until it reaches $T = 719$ K when the curve seems to become stationary as well. Not surprisingly, the physics ruling the temperature evolution of $\Gamma_{M_{11}}$ and $\Gamma_{M_{22}}$ is intimately connected to the physics we discussed explaining the IAs in Fig. 3(a). As explained above, the temperature dependence of the linewidths are well described in terms of $e-ph$ couplings [Eq. (6)] and $ph-ph$ couplings [Eq. (7)]. The contributions coming from $e-ph$ couplings are found negligible. From Eq. (6) it is understood that the dependence of $\Delta\Gamma_{e-ph}$ with temperature is not as strong as the dependence of $\Delta\Gamma_{e-ph}$ with the Fermi Level energy [10,14,27,28]. Therefore, $\Delta\Gamma_{ph-ph}$ [Eq. (7)] must be able to explain the $\Gamma_{M_{11}}$ and $\Gamma_{M_{22}}$ results. In fact, when $T < 543$ K it is expected that the three-phonon process dominates [2,5,12,23,58,61] and this is exactly what is observed. As mentioned earlier in the text, LOZO' is a combination of two phonons, and therefore, Eq. (7) must take into account three- and four-phonon processes for the LO phonon and three- and four-phonon processes for the ZO' phonon as well, which gives us a total of four parameters: D_{LO}^{3-ph} , $D_{ZO'}^{3-ph}$, D_{LO}^{4-ph} , and $D_{ZO'}^{4-ph}$. All possible combinations of parameters in Eq. (7) have been attempted to fit the data range when $T < 543$ K; success was found when four-phonon processes were disregarded [see Fig. S1(a) in the Supplemental Material (SM) [68]]. Both $\Gamma_{M_{11}}$ and $\Gamma_{M_{22}}$ increase monotonically with increasing temperature, which means that the lifetimes of the phonons involved (LO and ZO') are decreasing. This result is consistent with the literature [11,16,26,30], which reports that phonon lifetimes in carbon materials such as 1LG, 2LG, and graphite decrease with increasing temperature. Moreover, it supports the claim that the three-phonon relation process is efficient in this range of temperature. The linewidth is inversely proportional to the phonon lifetime and their connection is made by the Plank constant: $\Gamma_{M_{ii}} = \hbar/\gamma_{M_{ii}}$ ($i = 1,2$), in which $\gamma_{M_{ii}}$ is the phonon lifetime [see the inset in Fig. 3(b)] [1,65,66].

For $T \geq 543$ K, $\Gamma_{M_{11}}$ continues to monotonically increase but $\Gamma_{M_{22}}$ starts decreasing as the temperature increases, which means that $\gamma_{M_{11}}$ is still decreasing while $\gamma_{M_{22}}$ is now increasing. The results seen for $\Gamma_{M_{ii}}$ ($i = 1,2$) corroborate those results observed for the IAs. Since $\gamma_{M_{11}}$ is decreasing with increasing T , two conclusions can be reached: (1) the generation rates of phonons associated to the M_{11} peak are smaller than their relaxation rates (the relaxation of phonons is efficient), and (2) photoexcited electrons do not reach thermal equilibrium with phonons. On the other hand, $\Gamma_{M_{22}}$ is decreasing, which means that the phonon lifetime is increasing for those phonons participating on the processes involving the π_2^* band. Such an increase in the phonons' lifetimes is in good agreement with the stationary regime reached by the $IA_{M_{22}}$ and supports the explanations given above: it is well known that high-energy carriers (such as photoexcited electrons) decay first (and

faster) via creation of optical phonons and that optical phonons decay into acoustic phonons [1,2,5,9,11,16,23–26,30]. For $T \geq 543$ K, with the increase in the net relaxation of electrons from π_1^* to π_2^* via ZO' phonon emissions, many more electrons will be scattered to form the M_{22} peak and, therefore, more LO and ZO' phonons will be generated. If the rate of generation of LO and ZO' phonons becomes higher than the respective relaxation times, electrons and phonons will remain in thermal equilibrium and their lifetimes increase considerably, which agrees with the $\Gamma_{M_{22}}$ behavior. For $T \geq 543$ K, the four-phonon process become paramount to fit and explains both M_{11} and M_{22} as seen in Fig. 3(b) (gray and black solid lines). Interestingly, for $T \geq 719$ K the LOZO' $\Gamma_{M_{11}}$ seems to be reaching a limit from which it does not considerably vary anymore. In other words, the rate $\partial\Gamma_{M_{11}}/\partial T$ seems to be decreasing with increasing T , and consequently $\gamma_{M_{11}}$ seems to no longer decrease. On the other hand, $\Gamma_{M_{22}}$ stops decreasing with increasing T , which means that $\gamma_{M_{22}}$ stops increasing. This scenario is again fully consistent with the results discussed for the IAs. Indeed, with increasing T the relaxation and generation rates of phonons, in particular ZO' phonons, become more balanced and this would decrease the efficiency of the net $\pi_1^* \rightarrow \pi_2^*$ relaxations, which consequently diminishes any change in $\gamma_{M_{11}}$ and $\gamma_{M_{22}}$. The values of D_{LO}^{3-ph} , $D_{ZO'}^{3-ph}$, D_{LO}^{4-ph} , and $D_{ZO'}^{4-ph}$ associated with the combination LOZO', for $T < 543$ K and for $T \geq 543$ K, are shown in Table I in the SM [68].

C. LOZO' frequency variations ($\Delta\omega_{M_{11}}$ and $\Delta\omega_{M_{22}}$)

Figure 3(c) shows the frequency variations $\Delta\omega_{M_{11}}$ and $\Delta\omega_{M_{22}}$ with increasing the temperature. For temperatures below 543 K ($T < 543$ K) the three-phonon process is dominant and the data can only be fit via Eq. (3) if the four-phonon processes are disregarded [see Fig. S1(b) in the SM [68]]. This is in full agreement with the findings for $\Gamma_{M_{ii}}$. Interestingly, the slope $\partial\omega_{M_{11}}/\partial T$ observed for $\Delta\omega_{M_{11}}$ is different from the slope $\partial\omega_{M_{22}}/\partial T$ observed for the $\Delta\omega_{M_{22}}$. The phonon anharmonicities are characterized by the deformation potential and phonon-dependent Grüneisen parameter in materials [1] which are essentially the same for both M_{11} and M_{22} combination modes because they originate from the same phonons, and the only difference between them is the phonon momentum, for which $q_{M_{22}} < q_{M_{11}}$ as previously discussed. Therefore, one would expect the same behavior for both M_{11} and M_{22} . In order to understand why $\Delta\omega_{M_{11}}$ and $\Delta\omega_{M_{22}}$ have different slopes and behaviors, we must recall the physics governing the generation of the M_{11} and M_{22} peaks: (1) One electron is excited to the conduction band (either to the π_1^* or to the π_2^*). Next, the electron is scattered from π_i^* to π_i^* ($i = 1, 2$) in a AV process and then scattered back by generating two phonons in the system (one LO and one ZO'). These Raman-scattering events are related to the e - ph couplings that intermediate the scattering events. The ph - ph couplings are not important in determining the scattering magnitudes but the phonon population is [1,65,66]. Therefore, a simple conclusion is that the smaller the number of scattering events the smaller the phonon generation. (2) The lifetimes of the generated LO and ZO' phonons, which depend on their decay rate into lower energy phonons, determine $\gamma_{M_{ii}}$ ($i = 1, 2$). As described above, the temperature dependence of both lifetimes and frequencies will be ruled by three- and four-phonon processes [see Eq. (3) and Eq. (7)]. (3) Similar to

the $\Gamma_{M_{ii}}$ ($i = 1, 2$) case, e - ph couplings are not as important as ph - ph couplings to understand the anharmonic effects in the frequency [5,6,10,14,23,27,28,58,60]. With the statements (1), (2) and (3) in mind, the increasing difference between the $\Delta\omega_{M_{11}}$ and $\Delta\omega_{M_{22}}$ slopes with increasing temperature is understood as follows: the net electron relaxation in 2LG is from π_1^* to π_2^* . This means that more electronic $\pi_2^* \rightarrow \pi_2^*$ inelastic scattering events will take place, which increases the average phonon population participating in such scattering events. This increase in phonon population enhances $\Delta\omega_{M_{22}}$ with increasing the temperature.

Another important observation: in the range of temperatures $T < 543$ K the total shift of -19.2 cm^{-1} and -17.2 cm^{-1} is observed for $\Delta\omega_{M_{22}}$ and $\Delta\omega_{M_{11}}$, respectively. These shifts extend to -28.2 cm^{-1} and -23.2 cm^{-1} for $\Delta\omega_{M_{22}}$ and $\Delta\omega_{M_{11}}$ at temperatures $T \geq 543$ K. Recently, Popov *et al.* [55] proposed that the combination mode LOZO' is specifically the LO mode with symmetry E_{1u} (baptized LO⁽⁻⁾) combined with the ZO' mode. Note that due to interlayer interactions between the top and bottom layers in a 2LG, the LO mode splits into E_{1u} (out-of-phase vibrations of the layers) and E_{2g} (in-phase vibrations of the layers baptized LO⁽⁺⁾). Around the Γ point [60], the frequency shift for the LO⁽⁺⁾ with increasing T is about -11.0 cm^{-1} , while the frequency shift for the LO⁽⁻⁾ is about -19.0 cm^{-1} . In addition, studies by Giura *et al.* [60] and Kong *et al.* [9] point that the ZO' and ZA phonons, which are out-of phase and in-phase vibrations of the layers in a 2LG, become increasingly important to ph - ph couplings as the temperature increases and such phonons get away from the Γ point. Moreover, the four-phonon coupling between LO⁽⁻⁾ and the ZO' modes is much stronger than the four-phonon coupling between LO⁽⁺⁾ and the ZO' modes, meaning the four-phonon coupling becomes increasingly more important with increasing the temperature [60]. The magnitudes of both $\Delta\omega_{M_{11}}$ and $\Delta\omega_{M_{22}}$ with increasing T supports the assignment by Popov [55] and the combination LOZO' should read LO⁽⁻⁾ZO⁽⁺⁾ (or M_{11}) and LO⁽⁻⁾ZO⁽⁻⁾ (or M_{22}). To further support this assignment, temperature-dependent Raman-scattering measurements of the ZO' by Lui *et al.* [69] and Cong *et al.* [70] in the range of temperatures from 300 to 850 K show that the decrease in the ZO' frequency with increasing T is less than 5 cm^{-1} . This means that most of $\Delta\omega_{M_{ii}}$ comes from the LO mode. Additionally, these results suggest that temperature-dependent Raman spectroscopy could be used as a technique to help assign phonon combinations and overtones in materials.

Note that the scattering process ruling the M_{11} and M_{22} peaks will generate both LO⁽⁻⁾ and ZO' phonons. Therefore, the relaxation processes associated to the M_{11} and M_{22} combinations will involve the ZO' phonon, which decays fast mostly via three-phonon processes [11,16,25,26,69], and the LO⁽⁻⁾ phonon, which decays via three- and four-phonon processes, where the four-phonon process would mostly involve one ZO' phonon and two other acoustic phonons (likely ZA phonons [11,16,25,26]). For $T \geq 543$ K both $\Delta\omega_{M_{11}}$ and $\Delta\omega_{M_{22}}$ present an unexpected evolution with increasing the temperature. Contrarily to the $\Delta\omega_{M_{22}}$ and $\Delta\omega_{M_{11}}$ cases for $T < 543$ K, it is now paramount to consider the four-phonon process that has been discussed so that Eq. (3) is able to fit the data. The need for this inclusion is expected for higher temperatures, in agreement to the discussion for the linewidths $\Gamma_{M_{ii}}$ ($i = 1, 2$)

[9,11,16,23–26,30,60]. It is noticeable that for $T \geq 719$ K both $\Delta\omega_{M_{11}}$ and $\Delta\omega_{M_{22}}$ no longer change. As discussed earlier in the text, electron and phonon relaxations are more efficient for processes that involve phonon emissions in comparison with processes that involve phonon absorptions. These phonon relaxations must be understood as net relaxations and are already taking into account the rates with which electrons and phonons are emitted and absorbed. When the absorption and emission rates become similar, equilibrium may occur and the relaxation processes become inefficient, as explained before for Γ_{ii} ($i = 1, 2$). In fact, as the temperature increases, phonon absorption will become more efficient since now thermal excitation will increase the phonon population. Therefore, the higher the temperature, the higher the probability for happening not only relaxations but also generations of LO and ZO' phonons due to absorption of acoustic phonons, or due to absorption of one ZO' phonon and two other acoustic phonons (in the case of the four-phonon process). Also, at such temperatures, the electronic transitions $\pi_2^* \rightarrow \pi_1^*$ and $\pi_1^* \rightarrow \pi_2^*$ due to ZO' phonon reabsorption will become important as well. Therefore, with all these processes coming closer to equilibrium, changes in both $\Delta\omega_{M_{11}}$ and $\Delta\omega_{M_{22}}$ must no longer be observed. The extra resonance with the ZO' in the interband and intraband transitions certainly plays an important role in these second-order processes since such stationary tendencies are also suggested for the G' band [40] but it is not seen for first-order processes such as the G band as show in Fig. 4(d). Figure 4(d) shows the temperature evolution for the G -band Raman frequency shift $\Delta\omega_G$, while the insets in Fig. 4(d) show the temperature evolution for the G -band linewidth Γ_G and lifetime γ_G . The results for $\Delta\omega_G$, Γ_G , and γ_G are in good agreement with the literature [18,40,62]: the black solid line in Fig. 4(d) is the fitting result using the relation $\Delta\omega_G = \chi_G T$, where $\chi_G = 1.5 \times 10^{-2} \text{ cm}^{-1}/\text{K}$ is the G -band first-order temperature coefficient. The linewidth was fitted using Eq. (7), with $D_G^{3-ph} = 14.6 \text{ cm}^{-1}$ and $D_G^{4-ph} = 0$. The values of C_{LO}^{3-ph} , $C_{ZO'}^{3-ph}$, C_{LO}^{4-ph} , and $C_{ZO'}^{4-ph}$ associated to the combination $LOZO'$, for $T < 543$ K and for $T \geq 543$ K, are shown in Table II in the SM [68].

D. 2ZO overtone case

By turning the attention to Figs. 3(e) and 3(f), it is seen that the temperature-related changes in phonon linewidths ($\Gamma_{2ZO_{q=2k}}$ and $\Gamma_{2ZO_{q=0}}$) and frequencies ($\Delta\omega_{2ZO_{q=2k}}$ and $\Delta\omega_{2ZO_{q=0}}$) for the overtone 2ZO are very weak; almost negligible within the experiment's precision. These observations are very distinct from those discussed above for the combination $LOZO'$ and corroborates the 2ZO assignment given to this Raman feature [14]. As extensively discussed throughout the paper, the temperature-dependent phenomenon is mainly ruled by phonon anharmonicities (anharmonic $ph-ph$ couplings), which are characterized by the deformation potential and by the mode's Grüneisen parameter (δ_{mode}) [9,71,72]. The Grüneisen parameter has a strong influence on the probability of a phonon of frequency ω_{ph} to be scattered by other phonons (in other words, a phonon of frequency ω_{ph} to couple to other phonons). Indeed, such probability is proportional to δ_{mode}^2 , which makes δ_{mode} a good measure of phonon anharmonicity [9,71,72]. While the Grüneisen parameters around the Γ point for the

LO phonon mode [9] (δ_{LO}) and for the ZO' mode [9] ($\delta_{ZO'}$) are, respectively, 1.87 and between 2.5 and 3.8, the Grüneisen parameter around the Γ point for the ZO phonon mode [9] (δ_{ZO}) is between -0.1 and -0.15 . This means that δ_{ZO} is more than 90% smaller than δ_{LO} and $\delta_{ZO'}$ around the Γ point. Physically speaking, a positive δ_{mode} implies a decrease in ω_{ph} (the lattice constant increases), while a negative δ_{mode} implies an increase in ω_{ph} (the lattice constant decreases) [9,71,72]. Therefore, the phonon anharmonicities for the ZO mode must be very small, which agrees with the experiment reported here. In fact, the probability that a ZO phonon participates in a three-phonon or four-phonon scattering is proportional to $\delta_{ZO}^2 = 0.02$, which is very small and dramatically reduces the efficiency of the mode's response to changes in the temperature. It is interesting to recall that even though the $ph-ph$ couplings for the ZO mode are inefficient, the frequencies and linewidths could still change with changing temperature via $e-ph$ couplings. However, as explained by Araujo *et al.* [39], due to a lack of phonon and electron momenta conservation requirements, resonant $e-ph$ couplings that lead to changes in both frequency and linewidths with increasing temperature are unlikely to happen. This can be understood via symmetry arguments since the deformation potential mediating the $e-ph$ coupling related to the ZO mode, which is an antisymmetric interlayer vibration, is not expected to allow coupling of orthogonal electronic states since its vibration breaks the lattice symmetry. The lack of efficient scattering mechanisms ($ph-ph$ and $e-ph$ couplings) also explains why the integrated areas in Figs. 3(d) increase smoothly and with similar rates and overall behaviors. Finally, if this Raman feature was indeed the phonon combination mode $TO^{(+)}ZO'$ at the K point instead of the 2ZO overtone at the Γ point, as suggested by Popov [55], one should be able to observe significant changes in frequencies and linewidths with increasing temperature since both TO and ZO' modes present significant Grüneisen parameters at the K point (around 2.55 and -1.30 , respectively) [9]. The experiments reveal, however, that such temperature-dependent changes do not take place.

V. CONCLUSIONS

In summary, this paper addressed anharmonicities associated to the phonon combination mode $LOZO'$, involving the longitudinal-optical mode LO and the layer breathing mode ZO' , and the phonon overtone 2ZO (out-of-phase vibration of the layers) in AB -stacked bilayer graphene (2LG). Using temperature-dependent Raman-scattering measurements in a broad range of temperatures, the results show that the ZO' mode carries a fundamental role in the electron and phonon relaxations in this layered material, especially at temperatures above 543 K. Although the $LOZO'$ feature presents an anomalous behavior with increasing temperature, the 2ZO overtone does not show any clear dependence of its frequency and linewidth (and therefore, lifetime) with temperature, which is expected since the Grüneisen parameter for the ZO phonon is close to zero and the probability that a $ph-ph$ coupling happens is small. The measurement technique and discussions presented in the paper, with regard to electron and phonon relaxations, have the potential to be extended to any other multilayered structure that presents ZO' - and ZO-like phonon modes. It is important to notice that, because the $LOZO'$

peaks directly involve the ZO' phonon, they become a primary choice to understand the importance of the ZO' phonon in the relaxations of electrons and phonons in 2LG in contrast with previous understanding suggested elsewhere [40]. Finally, the results show how temperature-dependent Raman spectroscopy was used as an efficient technique to make phonon assignments in two-dimensional structures. Here it is shown that the $LOZO'$ combination mode is in fact $LO^{(-)}ZO'$ and that the $2ZO$ is a good assignment for the overtone observed.

ACKNOWLEDGMENTS

The author acknowledges the University of Alabama College of Arts and Sciences for the financial support through startup funds. The author acknowledges Dr. D. L. Mafra for helping to collect some of the experimental data that resulted in this work, Professor M. Dresselhaus (in memoriam) for helpful discussions, and Dr. S. V. Ulrich for proofreading the manuscript.

-
- [1] M. A. Stroschio and D. Mitra, *Phonons in Nanostructures* (Cambridge University Press, New York, 2001).
- [2] P. G. Klemens, Anharmonic decay of optical phonons, *Phys. Rev.* **148**, 845 (1966).
- [3] A. H. Castro Neto, F. Guinea, N. M. R. Peres, K. S. Novoselov, and A. K. Geim, The electronic properties of graphene, *Rev. Mod. Phys.* **81**, 109 (2009).
- [4] P. Avouris, Z. Chen, and V. Perebeinos, Carbon-based electronics, *Nat. Nanotechnol.* **2**, 605 (2007).
- [5] M. Balkanski, R. F. Wallis, and E. Haro, Anharmonic decay of optical phonons, *Phys. Rev. B* **28**, 1928 (1983).
- [6] K. Gao, R. Dai, Z. Zhang, and Z. Ding, Anharmonic effects in single-walled carbon nanotube, *J. Phys.: Condens. Matter* **19**, 486210 (2007).
- [7] J. K. Viljas and T. T. Heikkilä, Electron-phonon heat transfer in monolayer and bilayer graphene, *Phys. Rev. B* **81**, 245404 (2010).
- [8] P. R. Shaina, L. George, V. Yadav, and M. Jaiswal, Estimating the thermal expansion coefficient of graphene: The role of graphene-substrate interactions, *J. Phys.: Condens. Matter* **28**, 085301 (2016).
- [9] B. D. Kong, S. Paul, M. Buongiorno Nardelli, and K. W. Kim, First-principles analysis of lattice thermal conductivity in monolayer and bilayer graphene, *Phys. Rev. B* **80**, 033406 (2009).
- [10] S. Piscanec, M. Lazzeri, F. Mauri, A. C. Ferrari, and J. Robertson, Kohn Anomalies and Electron-Phonon Interactions in Graphite, *Phys. Rev. Lett.* **93**, 185503 (2004).
- [11] K. Kang, D. Abdula, D. G. Cahil, and S. Moonsub, Lifetimes of optical phonons in graphene and graphite by time-resolved incoherent anti-Stokes Raman scattering, *Phys. Rev. B* **81**, 165405 (2010).
- [12] M. Sendova, L. Datas, D. L. Mafra, and E. Flahaut, Micro-Raman scattering of selenium-filled double-walled carbon nanotubes: Temperature study, *J. Appl. Phys.* **105**, 094312 (2009).
- [13] L. M. Malard, D. C. Elias, E. S. Alves, and M. A. Pimenta, Observation of Distinct Electron-Phonon Couplings in Gated Bilayer Graphene, *Phys. Rev. Lett.* **101**, 257401 (2008).
- [14] P. T. Araujo, D. L. Mafra, K. Sato, R. Saito, J. Kong, and M. S. Dresselhaus, Phonon Self-Energy Corrections to Nonzero Wave-Vector Phonon Modes in Single-Layer Graphene, *Phys. Rev. Lett.* **109**, 046801 (2012).
- [15] H. Tang and I. P. Herman, Raman microprobe scattering of solid silicon and germanium at the melting temperature, *Phys. Rev. B* **43**, 2299 (1991).
- [16] B. Gao, G. Hartland, T. Fang, M. Kelly, D. Jena, H. Xing, and L. Huang, Studies of intrinsic hot phonon dynamics in suspended graphene by transient absorption microscopy, *Nano Lett.* **11**, 3184 (2011).
- [17] D. Yoon, Y.-W. Son, and H. Cheong, Negative thermal expansion coefficient of graphene measured by Raman spectroscopy, *Nano Lett.* **11**, 3227 (2011).
- [18] I. Calizo, A. A. Balandin, W. Bao, F. Miao, and C. N. Lau, Temperature dependence of the Raman spectra of graphene and graphene multilayers, *Nano Lett.* **7**, 2645 (2007).
- [19] Y. Magnin, G. D. Förster, F. Rabilloud, F. Calvo, A. Zapelli, and C. Bichara, Thermal expansion of free-standing graphene: benchmarking semi-empirical potentials, *J. Phys.: Condens. Matter* **26**, 185401 (2014).
- [20] J.-U. Lee, D. Yoon, H. Kim, S. W. Lee, and H. Cheong, Thermal conductivity of suspended pristine graphene measured by Raman spectroscopy, *Phys. Rev. B* **83**, 081419(R) (2011).
- [21] S. Chen, L. A. Moore, W. Cai, J. W. Suk, J. An, C. Mishra, C. Amos, C. W. Magnuson, J. Kang, L. Shi, and R. S. Ruoff, Raman measurements of thermal transport in suspended monolayer graphene of variable sizes in vacuum and gaseous environments, *ACS Nano* **5**, 321 (2011).
- [22] A. A. Balandin, Thermal properties of graphene and nanostructured carbon materials, *Nat. Mater.* **10**, 569 (2011).
- [23] W. S. Li, Z. X. Shen, Z. C. Feng, and S. J. Chua, Temperature dependence of Raman scattering in hexagonal gallium nitride films, *J. Appl. Phys.* **87**, 3332 (2000).
- [24] W.-K. Tse and S. Das Sarma, Energy relaxation of hot Dirac fermions in graphene, *Phys. Rev. B* **79**, 235406 (2009).
- [25] L. Lindsay, D. A. Broido, and N. Mingo, Flexural phonons and thermal transport in multilayer graphene and graphite, *Phys. Rev. B* **83**, 235428 (2011).
- [26] L. Huang, G. V. Hartland, L.-Q. Chu, Luxmi R. M. Feenstra, C. Lian, K. Tahy, and H. Xing, Ultrafast transient absorption microscopy studies of carrier dynamics in epitaxial graphene, *Nano Lett.* **10**, 1308 (2010).
- [27] N. Bonini, M. Lazzeri, N. Marzari, and F. Mauri, Phonon Anharmonicities in Graphite and Graphene, *Phys. Rev. Lett.* **99**, 176802 (2007).
- [28] M. Lazzeri, S. Piscanec, F. Mauri, A. C. Ferrari, and J. Robertson, Phonon linewidths and electron-phonon coupling in graphite and nanotubes, *Phys. Rev. B* **73**, 155426 (2006).
- [29] R. W. Newson, J. Dean, B. Schimidt, and H. M. van Driel, Ultrafast carrier kinetics in exfoliated graphene and thin graphite films, *Opt. Express* **14**, 2326 (2009).
- [30] S. Ulstrup, J. C. Johannsen, F. Cilent, J. A. Miwa, A. Crepaldi, M. Zacchigna, C. Cacho, R. Chapman, E. Springate, S. Mammadov, F. Fromm, C. Roidel, Th. Seyller, F. Parmigiani, M. Grioni, P. D. C. King, and P. Hofmann, Ultrafast Dynamics of Massive Dirac

- Fermions in Bilayer Graphene, *Phys. Rev. Lett.* **112**, 257401 (2014).
- [31] P. A. George, J. Strait, J. Dawlaty, S. Shivaraman, M. Chandrashekhara, F. Rana, and M. G. Spencer, Ultrafast optical-pump terahertz-probe spectroscopy of the carrier relaxation and recombination dynamics in epitaxial graphene, *Nano Lett.* **12**, 4248 (2008).
- [32] L. Ren, Q. Zhang, J. Yao, Z. Sun, R. Kaneko, Z. Yan, S. Nanot, Z. Jin, I. Kawayama, M. Tonouchi, J. T. Tour, and J. Kono, Terahertz and infrared spectroscopy of gated large-area graphene, *Nano Lett.* **12**, 3711 (2012).
- [33] J. H. Strait, H. Wang, S. Shivaraman, V. Shields, M. G. Spencer, and F. Rana, Very slow cooling dynamics of photoexcited carriers in graphene observed by optical-pump terahertz-probe spectroscopy, *Nano Lett.* **11**, 4902 (2011).
- [34] H. A. Hafez, X. Chai, Y. Sekine, M. Takamura, K. Oguri, I. Al-Naib, M. M. Dignam, H. Hibino, and T. Ozaki, Effects of environmental conditions on the ultrafast carrier dynamics in graphene revealed by terahertz spectroscopy, *Phys. Rev. B* **95**, 165428 (2017).
- [35] A. C. Ferrari, J. C. Meyer, V. Scardaci, C. Casiraghi, M. Lazzeri, F. Mauri, S. Piscanec, D. Jiang, K. S. Novoselov, S. Roth, and A. K. Geim, Raman Spectrum of Graphene and Graphene Layers, *Phys. Rev. Lett.* **97**, 187401 (2006).
- [36] R. Ma and T. Sasaki, Nanosheets of oxides and hydroxides: Ultimate 2D chargebearing functional crystallites, *Adv. Mater.* **22**, 5082 (2010).
- [37] K. S. Novoselov, D. Jiang, F. Schedin, T. J. Booth, V. V. Khotkevich, S. V. Morozov, and A. K. Geim, Two-dimensional atomic crystals, *Proc. Natl. Acad. Sci. USA* **102**, 10451 (2005).
- [38] H. O. H. Churchill and P. Jarillo-Herrero, Two-dimensional crystals: Phosphorus joins the family, *Nat. Nanotechnol.* **9**, 330 (2014).
- [39] P. T. Araujo, D. L. Mafra, K. Sato, R. Saito, J. Kong, and M. S. Dresselhaus, Unraveling the interlayer-related phonon self-energy renormalization in bilayer graphene, *Sci. Rep.* **2**, 1017 (2012).
- [40] D. L. Mafra, J. Kong, K. Sato, R. Saito, M. S. Dresselhaus, and P. T. Araujo, Using the G' Raman cross-section to understand the phonon dynamics in bilayer graphene systems, *Nano Lett.* **12**, 2883 (2012).
- [41] Y. Zhao, X. Luo, H. Li, J. Zhang, P. T. Araujo, C. W. Gan, J. Wu, H. Zhang, S. Y. Que, M. S. Dresselhaus, and Q. Xiong, Interlayer breathing and shear modes in few-trilayer MoS_2 and WSe_2 , *Nano Lett.* **13**, 1007 (2013).
- [42] C. H. Lui and T. F. Heinz, Measurement of layer breathing mode vibrations in few-layer graphene, *Phys. Rev. B* **87**, 121404(R) (2013).
- [43] C. H. Lui, L. M. Malard, S. Kim, G. Lantz, F. E. Laverge, R. Saito, and T. F. Heinz, Observation of layer-breathing mode vibrations in few-layer graphene through combination Raman scattering, *Nano Lett.* **12**, 5539 (2012).
- [44] N. B. Le, T. D. Huan, and L. M. Woods, Interlayer interactions in van der Waals heterostructures: Electron and phonon properties, *ACS Appl. Mater. Interfaces* **8**, 6286 (2016).
- [45] S. Huang, L. Liang, X. Ling, A. A. Puretzy, D. B. Geohegan, B. G. Sumpter, J. Kong, V. Meunier, and M. S. Dresselhaus, Low-frequency interlayer Raman modes to probe interface of twisted bilayer MoS_2 , *Nano Lett.* **16**, 1435 (2016).
- [46] L. Paulatto, F. Mauri, and M. Lazzeri, Anharmonic properties from a generalized third-order ab initio approach: Theory and applications to graphite and graphene, *Phys. Rev. B* **87**, 214303 (2013).
- [47] J. Jiang, R. Saito, A. Grüneis, G. Dresselhaus, and M. S. Dresselhaus, Electron-phonon interaction and relaxation time in graphite, *Chem. Phys. Lett.* **392**, 383 (2004).
- [48] K. M. Borysenko, J. T. Mullen, X. Li, Y. G. Semenov, J. M. Zavada, M. Buongiorno Nardelli, and K. W. Kim, Electron-phonon interactions in bilayer graphene, *Phys. Rev. B* **83**, 161402(R) (2011).
- [49] C.-H. Park, F. Giustino, M. L. Cohen, and S. G. Louie, Electron-phonon interactions in graphene, bilayer graphene, and graphite, *Nano Lett.* **8**, 4229 (2008).
- [50] P. T. Araujo, O. Frank, D. L. Mafra, W. Fang, J. Kong, M. S. Dresselhaus, and K. Martin, Mass-related inversion symmetry breaking and phonon self-energy renormalization in isotopically labeled AB-stacked bilayer graphene, *Sci. Rep.* **3**, 2061 (2013).
- [51] C. H. Lui, Z. Li, K. F. Mak, E. Cappelluti, and T. F. Heinz, Observation of an electrically tunable band gap in trilayer graphene, *Nat. Phys.* **7**, 944 (2011).
- [52] K. Sato, J. S. Park, R. Saito, C. Cong, T. Yu, C. H. Lui, T. F. Heinz, G. Dresselhaus, and M. S. Dresselhaus, Raman spectra of out-of-plane phonons in bilayer graphene, *Phys. Rev. B* **84**, 035419 (2011).
- [53] J.-A. Yan, W. Y. Ruan, and M. Y. Chou, Phonon dispersions and vibrational properties of monolayer, bilayer, and trilayer graphene: Density-functional perturbation theory, *Phys. Rev. B* **77**, 125401 (2008).
- [54] L. M. Malard, M. H. D. Guimarães, D. L. Mafra, M. S. C. Mazzoni, and A. Jorio, Group-theory analysis of electrons and phonons in N-layer graphene systems, *Phys. Rev. B* **79**, 125426 (2009).
- [55] V. N. Popov, Two-phonon Raman bands of bilayer graphene: Revisited, *Carbon* **91**, 436 (2015).
- [56] K. V. Zakharchenko, J. H. Los, M. I. Katsnelson, and A. Fasolino, Atomistic simulations of structural and thermodynamic properties of bilayer graphene, *Phys. Rev. B* **81**, 235439 (2010).
- [57] K. T. Nguyen, D. Abdula, C.-L. Tsai, and S. Moonsub, Temperature and gate voltage dependent Raman spectra of single-layer graphene, *ACS Nano* **5**, 5273 (2011).
- [58] L. Ci, Z. Zhou, X. Yan, D. Liu, H. Yuan, Y. Gao, J. Wang, L. Liu, W. Zhou, G. Wang, and S. Xie, Temperature dependence of resonant Raman scattering in double-wall carbon nanotubes, *Appl. Phys. Lett.* **82**, 3098 (2003).
- [59] M. J. Allen, J. D. Fowler, V. C. Tung, Y. Yang, B. H. Bruce, and R. B. Kaner, Temperature dependent Raman spectroscopy of chemically derived graphene, *Appl. Phys. Lett.* **93**, 193119 (2008).
- [60] P. Giura, N. Bonini, G. Creff, J. B. Brubach, P. Roy, and M. Lazzeri, Temperature evolution of infrared- and Raman-active phonons in graphite, *Phys. Rev. B* **86**, 121404(R) (2012).
- [61] S. Tian, Y. Yang, Z. Liu, C. Wang, R. Pan, C. Gu, and J. Li, Temperature-dependent Raman investigation on suspended graphene: Contribution from thermal expansion coefficient mismatch between graphene and substrate, *Carbon* **104**, 27 (2016).
- [62] I. Calizo, F. Miao, W. Bao, C. N. Lau, and A. A. Ballandin, Variable temperature Raman microscopy as a nanometrology

- tool for graphene layers and graphene-based devices, *Appl. Phys. Lett.* **91**, 071913 (2007).
- [63] A. K. Geim and K. S. Novoselov, The rise of graphene, *Nat. Mater.* **6**, 183 (2007).
- [64] L. M. Malard, J. Nilsson, D. C. Elias, J. C. Brant, F. Plentz, E. S. Alves, A. H. Castro Neto, and M. A. Pimenta, Probing the electronic structure of bilayer graphene by Raman scattering, *Phys. Rev. B* **76**, 201401(R) (2007).
- [65] H. Kuzmany, *Solid-State Spectroscopy: An Introduction*, 2nd ed. (Springer-Verlag, Berlin, 2009).
- [66] P. Y. Yu and M. Cardona, *Fundamentals of Semiconductors: Physics and Materials Properties*, 3rd ed. (Springer-Verlag, Berlin, 2005).
- [67] J. Jiang, R. Saito, Ge. G. Samsonidze, S. G. Chou, A. Jorio, G. Dresselhaus, and M. S. Dresselhaus, Electron-phonon matrix elements in single-wall carbon nanotubes, *Phys. Rev. B* **72**, 235408 (2005).
- [68] See Supplemental Material at <http://link.aps.org/supplemental/10.1103/PhysRevB.97.205441> for one figure and two tables with the values for the fitting parameters C_{mode}^{3-ph} , C_{mode}^{4-ph} , D_{mode}^{3-ph} , and D_{mode}^{4-ph} , for both LO and ZO' phonon modes participating in the phonon combination LOZO'. The figure shows the fitting results for $\Delta\omega_{M_{ii}}$ and $\Gamma_{M_{ii}}$ (for $i = 1, 2$) in the range of temperatures $300 \text{ K} < T < 543 \text{ K}$.
- [69] C. H. Lui, Z. Ye, K. Courtney, X. Xiao, and R. He, Temperature-activated layer-breathing vibrations in few-layer graphene, *Nano Lett.* **14**, 4615 (2014).
- [70] C. Cong and T. Yu, Enhanced ultra-low-frequency interlayer shear modes in folded graphene layers, *Nat. Commun.* **5**, 4709 (2014).
- [71] C. H. Lee and C. K. Gan, Anharmonic interatomic force constants and thermal conductivity from Grüneisen parameters: An application to graphene, *Phys. Rev. B* **96**, 035105 (2017).
- [72] J. P. Herermans, The anharmonicity blacksmith, *Nat. Phys.* **11**, 990 (2015).